JOURNAL OF MATERIALS SCIENCE 21 (1986) 411–418

Crack resistance curves of alumina and zirconia at room temperature

H. WIENINGER, K. KROMP*
Institut für Festkörperphysik, University of Vienna, A-1090 Vienna, Austria
R. F. PABST
Max-Planck-Institut für Metallforschung, Seestrasse 92, 7000 Stuttgart 1, Federal Republic of Germany

Ceramic three-point bend specimens were pre-cracked in a displacement-controlled test in air at room temperature to form sharp cracks of different lengths. Critical stress intensity factors (K_{IC}) were then measured as a function of sharp crack length in a fast-fracture, load-controlled test. Crack resistance curves (K_{IC} against crack length) were determined for three commercially pure aluminas of different grain size, a debased alumina containing a glassy phase, and a partially stabilized zirconia (PSZ) material. The crack resistance curves proved to be flat for the finer-grained and the debased alumina. A steeply rising crack resistance curve was, however, observed for a pure coarse-grained alumina material which is explained by friction effects of the cracked microstructure behind the measured crack front. The effect is influenced by the test procedure itself. Though crack branching takes place the crack resistance curve of PSZ is completely flat, which is attributed to fast fracture testing where only the most dangerous flaw is activated.

1. Introduction

Ceramic materials are normally completely brittle at room temperature. The brittleness implies that linear elastic fracture mechanics is best suited for fracture toughness measurements and subcritical crack extension characterization. It may be assumed that the fracture toughness value turns out to be a material constant independent of crack length.

In contradiction to these presumptions it was found in an earlier paper [1] that fracture toughness data measured with sharp cracks showed a strong dependence on crack length, in which the fracture toughness or crack resistance increases with increasing crack length.

The load–displacement records of the experiments leading to this dependency were performed in a more or less controlled manner, and showed increasingly non-linear behaviour with increasing sharp, natural crack lengths [2].

In analogy with plasticity reactions with metallic materials the effect was first explained by a "process zone" of microcracking *ahead* of the actual crack tip, the size of the microcracks being typically of the order of the structural element (i.e. the grain size). The rising crack resistance curve was then explained by an enlargement of this "process zone" with increasing crack length, in complete analogy with the increase in the size of the plastic zone found in metallic materials.

However, as a "process zone" could not be detected [2] it was then alternatively argued [1, 2] that friction effects or adhesive forces at the crack surfaces *behind* the actual crack tip cause the unusual behaviour. These arguments were supported by measurements with narrow notches which guarantee traction-free crack surfaces. It could be proved that crack resistance curves measured with narrow notches are completely flat [1] (Fig. 1). Meanwhile similar behaviour was found by other authors [3–6] and a broad discussion has developed about the pre-conditions and the nature of this strange phenomenon.

The existence or non-existence of a rising crack resistance curve has very important practical consequences: the question is whether a single fracture toughness parameter is sufficient to characterize catastrophic failure or if a crack resistance curve is neces-

As mentioned above, the fracture toughness data (as a function of crack length) were evaluated from more or less subcritical, displacement-controlled tests which can cause crack branching and microcrack formation. If fracture toughness should characterize the catastrophic failure in a linear elastic test, then rapid, load-controlled experiments should be performed, as in the present work. Nevertheless, sharp cracks of distinct lengths have to be introduced by a displacement-controlled subcritical test procedure.

For the experiments a variety of materials were chosen with different tendencies towards secondary crack formation and microcracking.

2. Experimental procedure

The K_r curves were determined as listed below.

2.1. The precracking process

Three-point bend specimens 7 mm × 2.5 mm ×

Present address: Max-Planck-Institute für Metallforschung, Seestrasse 92, 7000 Stuttgart 1, Federal Republic of Germany.

0022–2461/86 $03.00 + .12

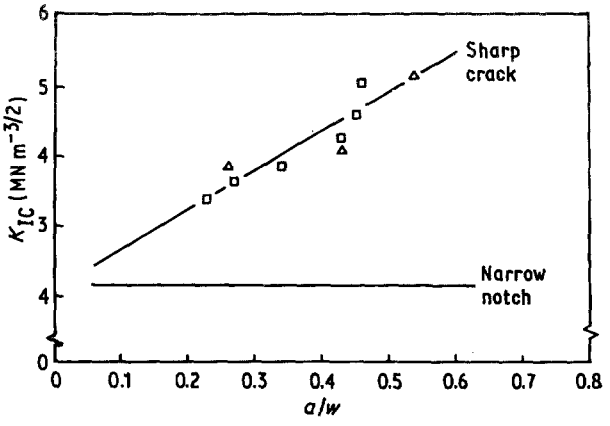

Figure 1 K_{IC} values for Al_2O_3, measured with sharp cracked and notched specimens [1].

40 mm in size (span width 30 mm) were notched to a normalized notch depth of 0.2 and then pre-cracked to the desired natural crack length in a displacement-controlled test in air at room temperature. The displacement rate of 1 μm min^{-1} promotes crack branching and microcracking. After the desired sharp crack length was reached the specimens were unloaded. The displacement-controlled test was made possible by using an extremely stiff bending device with SiC supports together with a stiff testing machine of very low compliance $C_m = 0.0109 \pm 0.0003$ μm N^{-1}. The displacement was directly measured and controlled by a linear voltage differential transformer in contact with the lower specimen surface.

2.2. Crack length measurement

As there is no macroscopic blunting effect with ceramic materials the actual crack tip is hard to detect. The cracked surfaces are close together, which enhances friction effects behind the crack tip. Therefore special attention has to be given to measuring crack lengths and crack elongation during and after the pre-cracking process.

Three methods were used:

(a) Side-light technique (Fig. 2). The crack lengths were measured after pre-cracking and unloading in a microscope on both polished sides of the specimen.

(b) Post-test investigation (Fig. 3). After the fast fracture test the cracked surfaces were investigated. A transition from inter-granular to trans-granular fracture was detected which separates the precracking region from the load-controlled, fast-fracture toughness test region. The pre-crack front was always found to be straight.

(c) Direct, visual observation (Fig. 4). The pre-cracking process was directly observed with a travelling microscope at a magnification of $\times 250$ [7]. With direct observation the crack length could be measured while the specimen was under load. This method facilitates detection of the crack tip. The kinetics of crack growth, secondary crack formation, crack branching and microcracking may also be observed using this technique.

The specimens were polished but not etched, as the width of the grain boundaries is of the same dimension as the distance of the cracked surfaces near the crack tip. Table I shows crack length values for two examples, measured using the three different methods. There is no significant difference between the results of the three evaluation methods. The mean scatter in crack length was found to be about 3%.

2.3. The crack resistance curve

The pre-cracked specimens were rapidly loaded to fracture in a load-controlled test at a loading rate of 100 N sec^{-1}. Thus subcritical crack extension was avoided and a true critical test was performed. The fracture toughness K_{IC} was then calculated using the linear elastic equation

$$K_{IC} = \tfrac{3}{2} \frac{P_c S}{BW^2} a_c^{1/2} Y(a/W) \qquad (1)$$

where P_c = critical load, S = span, B = specimen thickness, W = specimen width, a_c = critical total crack length (notch length + sharp crack length), $Y(a/W)$ = correction function [8].

The K_{IC} data are plotted against the total normalized crack lengths a/W, producing the K_R curve. Equation 1 implies that the cracked surfaces are stress-free or traction-free, where a_c is the crack length measured. Equation 1 does not account for friction effects and adhesive forces behind the measured crack tip. Traction-free surfaces are certainly guaranteed if narrow notches instead of sharp, natural cracks are used.

3. Materials

Four alumina materials of different grain size and purity were used. Three were commercially pure; the fourth, Al_2O_3–S, was of a debased quality with a glassy phase content of about 3 wt % SiO_2 (Table II).

It is well known that the internal stresses of alumina materials increase with increasing grain size. Therefore microcracking and secondary crack formation, and thus the capability for energy dissipation

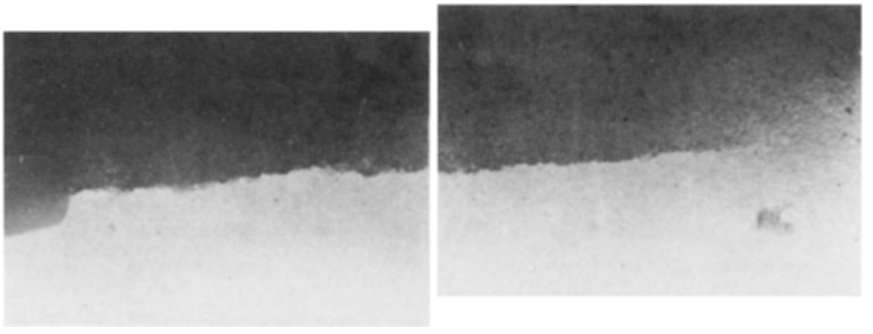

Figure 2 Crack length measurement by side-light technique.

TABLE I Comparison of crack length measurements

Examples for scatter	Crack length (mm)			
	Direct observation	Side-light technique	Fracture surface observation	Mean value
Mean (Specimen 36I)	2.282	2.432	2.398	2.371 ± 3.3%
Maximum (Specimen 57I)	2.367	2.688 2.528	2.807 2.749	2.626 ± 6.8%

TABLE II Properties of materials

Material	Composition (wt %)	Grain size (μm)	Young's modulus, 20° (GPa)	Density ($kg\,m^{-3}$)
Al_2O_3	97% Al_2O_3 + 3% SiO_2	9 to 11	360	3.82
Al_2O_3–fg	99.7% Al_2O_3 + 0.3% MgO	1	378	3.94
Al_2O_3–bio	99.8% Al_2O_3 + 0.2% MgO	3	391	3.95
Al_2O_3–Al 23	99.6% Al_2O_3 + 0.4% MgO	20 to 40	350	3.87
ZrO_2–PSZ	Ca + MgO stabilized, 10 vol % tetragonal	60	210	5.75

should be enhanced with larger grains. In this sense Al_2O_3–Al 23 has a greater capability for microcrack formation than (e.g.) Al_2O_3–fg.

The glassy-phase material is thought to have less tendency to crack branching, as the second phase and the comparatively smaller grains prevent high internal stresses.

The partially stabilized zirconia ZrO_2–PSZ contains about 10 vol % tetragonal phase, which is transformed to monoclinic phase when the crack elongates (stress-induced transformation [9]). This zirconia material has large grains of nearly 60 μm diameter and has been found to be susceptible to crack branching [10]. Furthermore, the volume change after transformation should induce compression forces at the cracked surfaces. In a subcritical displacement-controlled test the material exhibits non-linear stress–strain behaviour [10], which is similar to the behaviour of coarse-grained alumina.

4. Results

The K_R curve (K_{IC} against a/W) referring to a more fine-grained alumina material Al_2O_3–bio (Table I), Fig. 5, shows a linear dependency on measured fracture toughness as a function of normalized crack length a/W. The straight line, obtained by regression, remains nearly horizontal at a slope of 0.13. The mean fracture toughness of $K_{IC} = 4.1 \pm 0.8\,MPa\,m^{1/2}$ is in good agreement with values obtained using narrow notches (notch root radius $\varrho \leqq 60\,\mu m$) where the surfaces are completely traction-free [11].

The regression line of Al_2O_3–fg (Fig. 6) shows a slope of only 0.68. The crack resistance curve may therefore be considered flat. On omitting the fracture toughness data for $a/W > 0.9$ the slope is even lowered to 0.34. As the correction function rises steeply to infinity if a/W approaches unity, small errors in crack length measurement lead to large errors in K_{IC} for $a/W > 0.9$. This explains the large scatter at high a/W values. For illustration, error bars and the Y function are drawn in Fig. 6. The mean K_{IC} value of $4.5 \pm 0.5\,MPa\,m^{1/2}$ is in good agreement with data obtained using narrow notches (Fig. 6), shown by open symbols; in all the diagrams the error bars for the K_{IC} measurements with notched specimens are of the size of the diameter of the symbols.

In contrast with the results above for comparatively fine-grained alumina materials, a steeply rising K_R curve was measured for the coarse-grained Al_2O_3–Al 23 (Fig. 7). The results correspond to pronounced

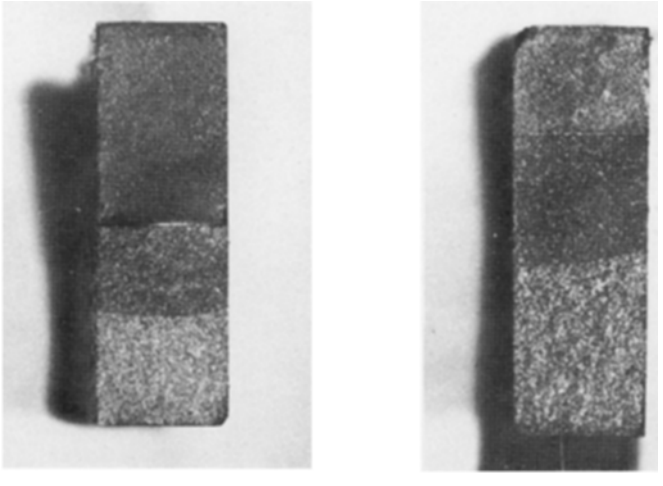

Figure 3 Transition from inter-granular to trans-granular fracture surface appearance.

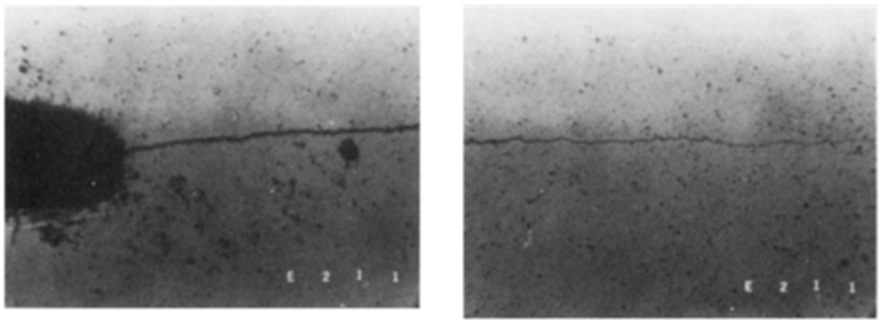

Figure 4 Crack length measurement by direct visual observation and photography.

non-linear stress–strain behaviour during the subcritical precracking process. Using the traction-free linear-elastic Equation 1, the fracture toughness value increases from $K_{IC} = 2.3\,MPa\,m^{1/2}$ at $a/W = 0.3$ (which is low) up to $10\,MPa\,m^{1/2}$ at $a/W = 0.9$, which is extremely high for alumina materials.

The broken line in Fig. 7 compares the results of a subcritical displacement-controlled test (displacement rate $3\,\mu m\,min^{-1}$) [12] with those of the critical test procedure used in Fig. 7 (closed symbols). Obviously the quality of a steeply rising crack resistance curve remains the same. The data for the critical test are usually located beneath the subcritical ones, indicating an effect of loading rate and different activating processes depending on the test procedure. For the present case the curves seem to be identical.

Notching the Al_2O_3–Al 23 specimens results in a completely flat K_R curve (open symbols in Fig. 7). This gives a strong indication that the steep rise of the K_R curve may be due to friction effects behind the actual crack front. The mean traction-free K_{IC} value of notched specimens was about $3\,MPa\,m^{1/2}$, which is somewhat lower than the data for the fine-grained alumina materials.

The K_R curve of the debased alumina Al_2O_3–S is given in Fig. 8. The slope of the regression line is only 0.61. This K_R curve may also be considered flat. The mean fracture toughness scatters about $3\,MPa\,m^{1/2}$ and exhibits (somewhat) lower values than that measured with narrow notches. Obviously the Al_2O_3–S is more notch-sensitive than the commercially pure materials, and the notch root radius used ($\varrho \leqq 60\,\mu m$) may be somewhat too large to simulate natural sharp cracks [13].

The crack resistance behaviour of the PSZ material is shown in Fig. 9. The curve remains completely flat, though crack branching (distinct single long cracks) was found [10] (Fig. 10). The mean fracture toughness of the pre-cracked specimens was $4.8\,MPa\,m^{1/2}$, which is nearly identical to data measured from notched ones ($4.9 \pm 0.1\,MPa\,m^{1/2}$). The results are surprising, as crack branching and transformation-induced internal stresses should result in friction effects and energy dissipation processes, so that behaviour similar to Al_2O_3–Al 23 would be anticipated.

5. Discussion

It is obvious from the results above that the existence or non-existence of a rising crack resistance curve measured in a critical test procedure depends on the type of microstructural features present. Increasing the grain size in alumina materials increases the internal stresses and the potential for microcracking and secondary crack formation. This may lead to a higher degree of energy dissipation. Damage during crack growth was therefore found especially in the coarse-grained Al_2O_3–Al 23 material. This behaviour prompted a more detailed post-test fracture surface investigation.

Fig. 11 shows the fracture surfaces of the Al_2O_3–bio material which has a fine-grained microstructure. Fig. 11a shows the area of slow crack growth (pre-cracking process), Fig. 11b the area near to the crack tip and

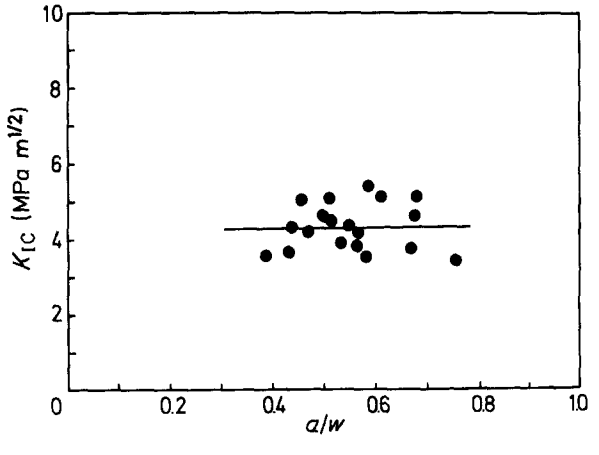

Figure 5 K_R curve for fine-grained pure alumina Al_2O_3–bio: sharp pre-cracking and fast fracture in air at room temperature (20° C). The straight line has a slope of 0.13.

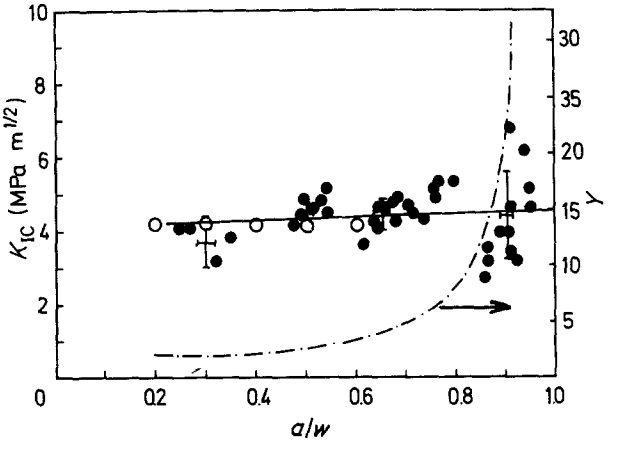

Figure 6 K_R curves for fine-grained alumina Al_2O_3–fg: sharp pre-cracking and fast fracture of pre-cracked and notched specimens in air at room temperature (20° C). (●) pre-cracked, (○) notched specimens; (—) K_R for slope 0.34; (— · —) correction function Y.

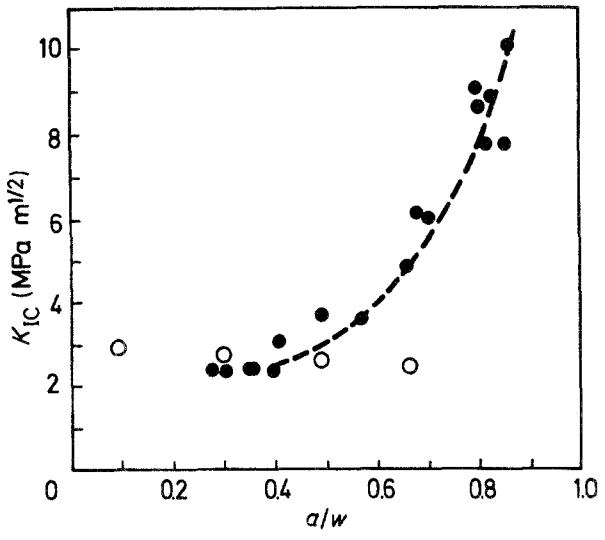

Figure 7 K_R curves for coarse-grained alumina Al_2O_3–Al 23 in air at room temperature (20° C): sharp pre-cracking and fast fracture of pre-cracked and notched specimens, and for comparison sharp cracking and displacement-controlled loading [12]. (●) K_R, critical test; (○) K_{IC}, notched specimen; (— — —) K_R, subcritical test.

Fig. 11c the area of fast crack growth in a K_{IC} test. A more intergranular fracture surface appearance is found for the lower crack velocity (pre-cracking), whereas the fracture seems to be more transgranular at high crack velocities. A distinct transition region is obvserved (Fig. 11b).

In contrast the fracture surfaces of Al_2O_3–Al 23 (Fig. 12a, area of slow crack growth; Fig. 12b, area of fast crack growth) look crushed and split. These phenomena are confirmed by observations of the crack path on the polished specimen surfaces [12] (Fig. 13).

It is important to note that some kind of "process zone" developing at the measured crack tip, which could explain the rising crack resistance curve, was not detected. It is much more likely that the damaged material behind the actual crack tip causes friction effects which, with increasing crack length, may increase and dissipate energy.

The traction-free relation of Equation 1 is no longer suitable, if friction effects or adhesive forces are act-

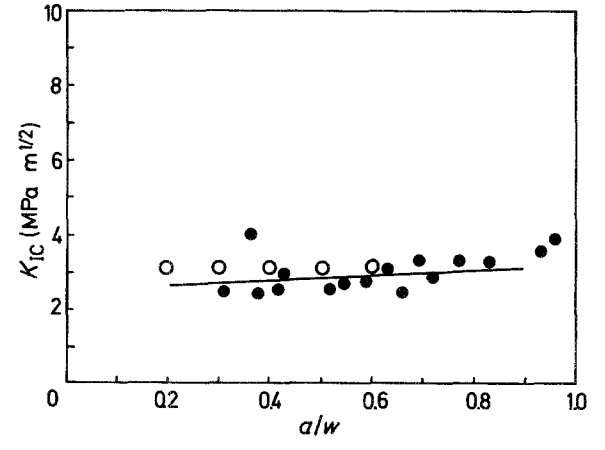

Figure 8 K_R curves for debased alumina Al_2O_3–S: sharp pre-cracking and fast fracture of pre- cracked and notched specimens in air at room temperature (20° C). (●) K_R; (—) K_R, slope 0.61; (○) K_{IC}, notched specimen.

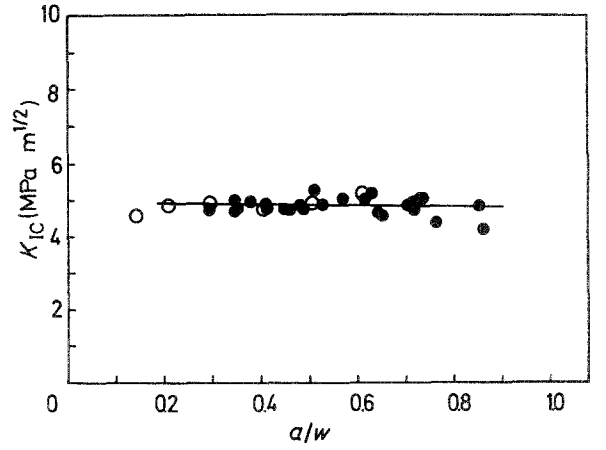

Figure 9 K_R curves for partially stabilized zirconia ZrO_2–PSZ: sharp pre-cracking and fast fracture of pre-cracked and notched specimens in air at room temperature (20° C). (●) K_R; (—) K_R, slope 0.13; (●) K_{IC}, notched specimen.

ing. It may simply and formally be replaced, using a procedure well established for metallic materials, by an expression for an effective stress intensity $K_{IC\,eff}$ defined with an effective crack length a_{eff} [15]:

$$a_{eff} = a_0 + d$$
$$K_{IC\,eff} = \sigma_c a_{eff}^{1/2} Y \quad (2)$$

where a_0 is the measured critical crack length and d the characteristic size of a friction zone behind the measured crack front, which in this case has to be subtracted and may increase with increasing sharp crack length.

It should be mentioned that in cases where crack branching and secondary crack formation occur, and in cases where the actual crack tip is hard to detect (there is no macroscopic crack tip blunting), defining and measuring an effective crack length will be difficult but decisive.

Nevertheless, displacement-controlled experiments with direct observation and measurement of crack extension allowed for a first rough evaluation of the size of this friction zone [7, 16].

For the measurements above it can be unambiguously stated that fine-grained alumina materials have flat K_R curves which are attributable to stress-free fracture surfaces. Materials with larger grains promote microcracking and crack branching, causing friction effects behind the crack front which result in a rising K_R curve if Equation 1 is used.

Referring to the literature [6, 10] and to Fig. 10, a rising K_R curve is also to be expected for the PSZ material. As visible from the fracture surfaces (Fig. 14), crack branching in the slow crack-growth area is apparent. It was surprising therefore that the K_R curve remained completely flat.

There are indications that for the PSZ material crack branching in the form of isolated large cracks exists, rather than a completely crushed region [10]. Perhaps this behaviour is influenced by a glassy phase at the grain boundaries. It may then be assumed that the fast-fracture test activates only the most dangerous flaw and diminishes the capability for energy dissipation.

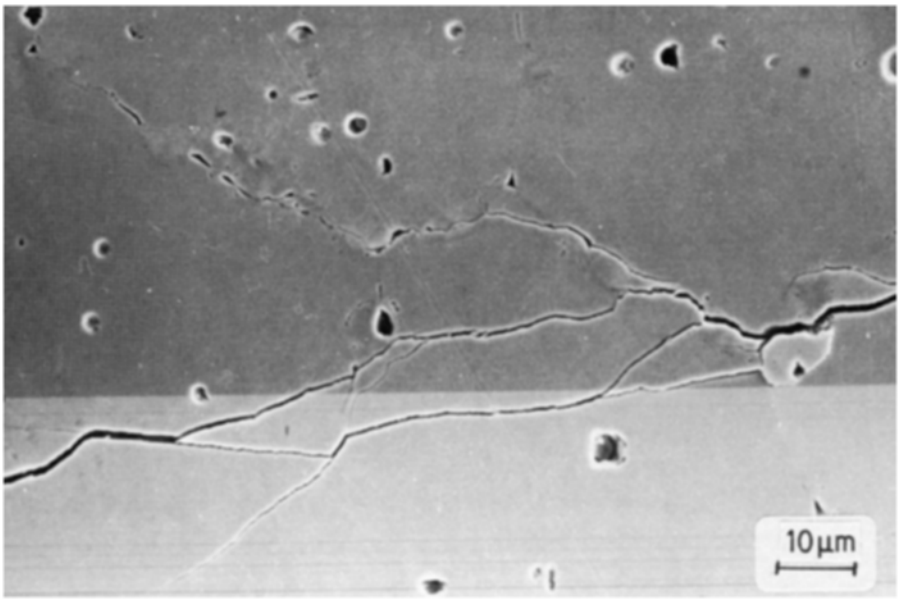

Figure 10 Crack-branching in zirconia ZrO_2–PSZ at room temperature [14].

Finally, for the debased alumina material Al_2O_3–S the completely flat K_R curve and the lack of any crack branching is mostly attributable to the glassy phase at grain boundaries, which is thought to reduce internal stresses during fabrication.

6. Summary and conclusion

K_R curves measured in a load-controlled critical fracture test with ceramic materials are normally horizontal. The K_{IC} data are practically identical with those measured with narrow notches. The fracture surfaces may therefore be assumed traction-free as is the case with notches, and Equation 1 may be used.

Amongst the five materials tested a coarse-grained alumina constituted an exception. It is assumed that in this material high internal stresses lead to enhanced microcracking and overall damage of the microstructure. A process or microcracking zone in front of the actual crack tip could not be detected. The energy dissipation processes could be confined mostly to a zone of destruction d behind the actual crack tip. This zone enlarges with increasing crack length. In this case a rising crack resistance cruve is measured independent of the experimental procedure of loading, whether subcritical displacement-controlled or critical load-controlled. If crack branching and secondary crack formation occur it is difficult to define a crack length. It is thought that this may be one of the main obstacles to obtaining reliable fracture toughness values.

The PSZ material, which also shows crack branching during the precracking process, has a completely flat K_R curve. It is thought (as the overall damage to the microstructure is much less than for the

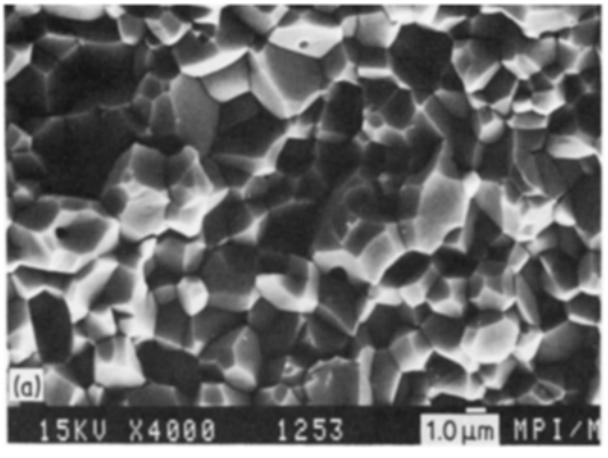

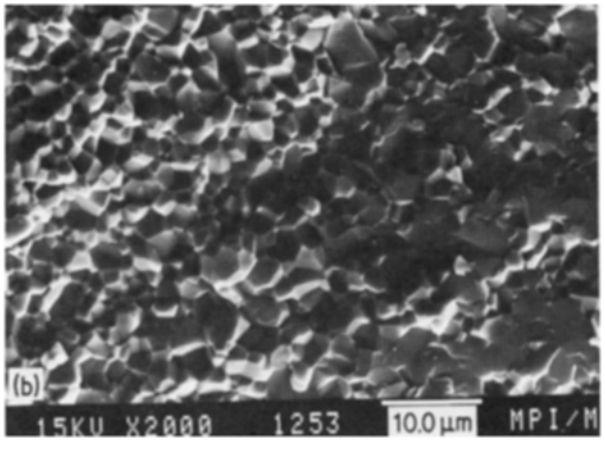

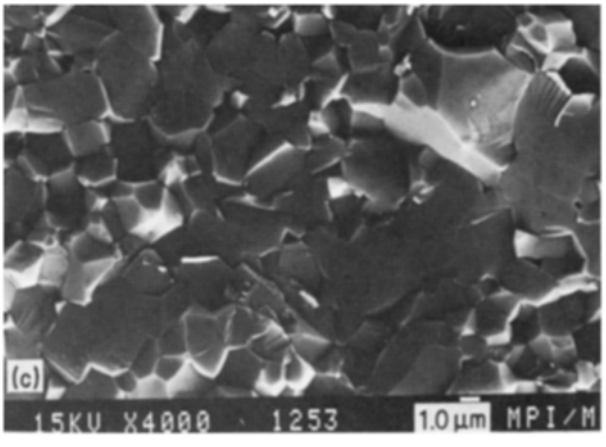

Figure 11 Fracture surface appearance of alumina Al_2O_3–bio: (a) area of slow crack growth, (b) transition region at crack front, (c) area of fast crack growth.

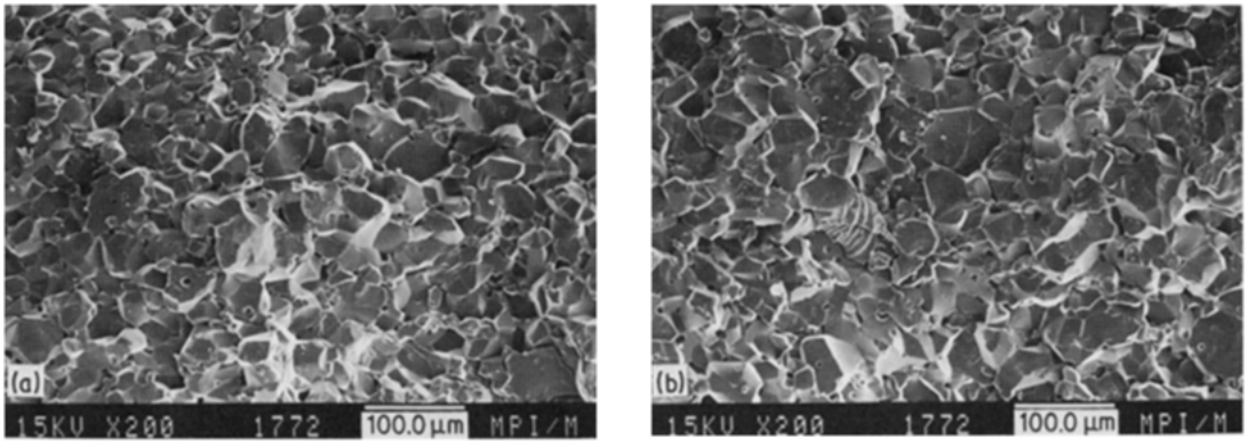

Figure 12 Fracture surface apppearance of alumina Al_2O_3–Al 23: (a) area of slow crack growth, (b) area of fast crack growth.

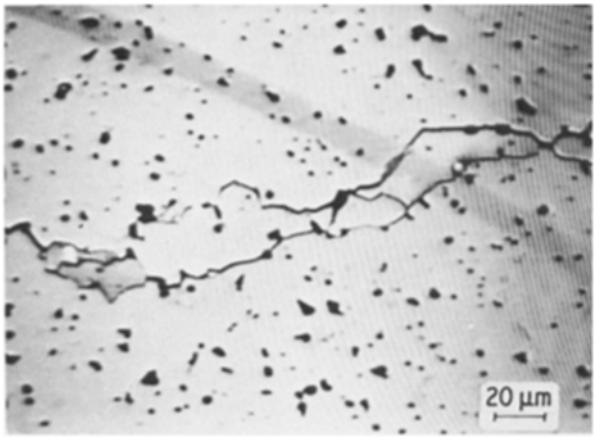

Figure 13 Crack path on the surface of Al_2O_3–Al 23 [12].

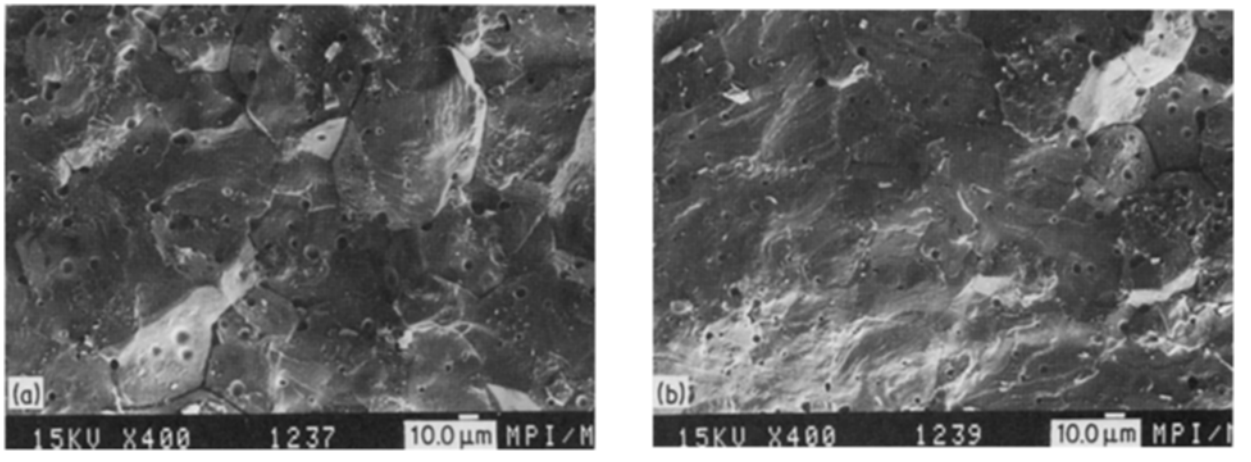

Figure 14 Fracture surface appearance of zirconia ZrO_2–PSZ: (a) area of slow crack growth, (b) area of fast crack growth.

coarse-grained alumina) that in a critical test only the most dangerous flaw is activated.

References

1. R. F. PABST, J. STEEB and N. CLAUSSEN "Fracture Mechanics of Ceramics," Vol. 4 edited by R. C. Bradt, D. P. H. Hasselman, and F. F. Lange (Plenum Press, New York, 1978) p. 821.
2. U. KROHN, PhD thesis, University of Stuttgart (1979).
3. F. W. KLEINLEIN, *Fortschr. Ber. (Verein Deutscher Ingenieure – Zeitschrift)* **18** (1980) 33.
4. Z. HUEBNER and W. JILECK, *J. Mater. Sci* **12** (1977) 117.
5. R. STEINBRECH, R. KNEHANS and W. SCHAARWÄCHTER, *ibid.* **18** (1983) 265.
6. R. H. J. HANNINK and M. U. SWAIN, *J. Aust. Ceram. Soc.* **18** (1982) 53.
7. A. C. BORNHAUSER, K. KROMP and R. F. PABST, *J. Mater. Sci.* **20** (1985) 2586.
8. J. E. SRAWLEY, *Int. J. Fract.* **12** (1976) 475.
9. LI SHING LI and R. F. PABST, *J. Mater. Sci.* **15** (1980) 2861.
10. W. VOGEL and R. F. PABST, Proceedings of 2nd International Conference on Creep and Fracture of Engineering Materials and Structures, Pineridge, Swansea, England, 1984, Part I, p. 485.

11. A. C. BORNHAUSER, Master thesis, University of Vienna (1980).
12. T. HAUG, private communication (1983).
13. R. F. PABST, "Fracture mechanics of Ceramics," Vol. 2, edited by R. C. Bradt, D. P. H. Hasselman and F. F. Lange (Plenum, New York, 1978) p. 555.
14. W. VOGEL, private communication (1983).
15. D. S. DUGDALE, *J. Mech. Phys. Solids* **18** (1960) 100.
16. T. HAUG, PhD thesis, University of Stuttgart (1985).

Received 5 October 1984
and accepted 25 February 1985